Initial validation of ozone measurements from the High Resolution Dynamics Limb Sounder

Bruno Nardi, John C. Gille, John J. Barnett, Cora E. Randall, V. Lynn Harvey, Alison Waterfall, W. Jolyon Reburn, Thierry Leblanc, Tom J. Mcgee, Laurence W. Twigg, et al.

Initial validation of ozone measurements from the High Resolution Dynamics Limb Sounder

Bruno Nardi,[1] John C. Gille,[1,2] John J. Barnett,[3] Cora E. Randall,[4] V. Lynn Harvey,[4] Alison Waterfall,[5] W. Jolyon Reburn,[5] Thierry Leblanc,[6] Tom J. McGee,[7] Laurence W. Twigg,[7] Anne M. Thompson,[8] Sophie Godin-Beekmann,[9] Peter F. Bernath,[10,11] Bojan R. Bojkov,[7] Chris D. Boone,[10] Charles Cavanaugh,[1] Michael T. Coffey,[1] James Craft,[2] Cheryl Craig,[1] Vincil Dean,[2] Thomas D. Eden,[1] Gene Francis,[1] Lucien Froidevaux,[12] Chris Halvorson,[1] James W. Hannigan,[1] Christopher L. Hepplewhite,[3] Douglas E. Kinnison,[1] Rashid Khosravi,[1] Charlie Krinsky,[2] Alyn Lambert,[12] Hyunah Lee,[1] Joanne Loh,[2] Steven T. Massie,[1] I. Stuart McDermid,[6] Daniel Packman,[1] Brendan Torpy,[2] Jessica Valverde-Canossa,[13] Kaley A. Walker,[10,14] David N. Whiteman,[7] Jacquelyn C. Witte,[15] and Greg Young[2]

Received 16 April 2007; revised 5 November 2007; accepted 28 December 2007; published 10 June 2008.

[1] Comparisons of the latest High Resolution Dynamics Limb Sounder (HIRDLS) ozone retrievals (v2.04.09) are made with ozonesondes, ground-based lidars, airborne lidar measurements made during the Intercontinental Chemical Transport Experiment–B, and satellite observations. A large visual obstruction blocking over 80% of the HIRDLS field of view presents significant challenges to the data analysis methods and implementation, to the extent that the radiative properties of the obstruction must be accurately characterized in order to adequately correct measured radiances. The radiance correction algorithms updated as of August 2007 are used in the HIRDLS v2.04.09 data presented here. Comparisons indicate that HIRDLS ozone is recoverable between 1 and 100 hPa at middle and high latitudes and between 1 and 50 hPa at low latitudes. Accuracy of better than 10% is indicated between 1 and 30 hPa (HIRDLS generally low) by the majority of the comparisons with coincident measurements, and 5% is indicated between 2 and 10 hPa when compared with some lidars. Between 50 and 100 hPa, at middle and high latitudes, accuracy is 10–20%. The ozone precision is estimated to be generally 5–10% between 1 and 50 hPa. Comparisons with ozonesondes and lidars give strong indication that HIRDLS is capable of resolving fine vertical ozone features (1–2 km) in the region between 1 and 50 hPa. Development is continuing on the radiance correction and the cloud detection and filtering algorithms, and it is hoped that it will be possible to achieve a further reduction in the systematic bias and an increase in the measurement range downward to lower heights (at pressures greater than 50–100 hPa).

Citation: Nardi, B., et al. (2008), Initial validation of ozone measurements from the High Resolution Dynamics Limb Sounder, *J. Geophys. Res.*, *113*, D16S36, doi:10.1029/2007JD008837.

[1]National Center for Atmospheric Research, Boulder, Colorado, USA.
[2]Center for Limb Atmospheric Sounding, University of Colorado, Boulder, Colorado, USA.
[3]Department of Physics, University of Oxford, Oxford, UK.
[4]Laboratory for Atmospheric and Space Physics, Boulder, Colorado, USA.
[5]Rutherford Appleton Laboratory, Didcot, UK.
[6]Table Mountain Facility, Jet Propulsion Laboratory, California Institute of Technology, Wrightwood, California, USA.
[7]NASA Goddard Space Flight Center, Greenbelt, Maryland, USA.
[8]Department of Meteorology, Pennsylvania State University, University Park, Pennsylvania, USA.
[9]Service d'Aéronomie/IPSL, CNRS, Université Pierre et Marie Curie, UMR 7620, Service d'Aéronomie, Paris, France.
[10]Department of Chemistry, University of Waterloo, Waterloo, Ontario, Canada.
[11]Department of Chemistry, University of York, Heslington, UK.
[12]Jet Propulsion Laboratory, Pasadena, California, USA.
[13]Laboratorio de Quimica de Atmosfera, Universidad Nacional, Heredia, Costa Rica.
[14]Department of Physics, University of Toronto, Toronto, Ontario, Canada.
[15]Science Systems and Applications, Inc., Lanham, Maryland, USA.

0148-0227/08/2007JD008837

1. Introduction

[2] HIRDLS measures ozone via three of its 21 infrared channels (numbers 10, 11, 12), with spectral centers at approximately 1000 cm^{-1}, 1030 cm^{-1}, and 1130 cm^{-1}, respectively, and which have responsivity full widths at half maximum of 20 cm^{-1}, 37 cm^{-1}, and 20 cm^{-1}, respectively [*Edwards et al.*, 1995]. The design sounding range of channel 10 is 8–75 km, and those of channels 11 and 12 are 30–85 km and 8–55 km, respectively [*Gille and Barnett*, 1996].

[3] A major issue in the reduction of data to geophysical parameters has been an unanticipated large visual obstruction in the HIRDLS field of view. After extensive analysis, it became apparent that a large piece of thermal insulating blanket from within the optical cavity ripped during the Aura spacecraft launch, owing to rapid decompression coupled with large g-forces and apparent inadequate venting, and moved into the optical path. This left an unobstructed optical path, at an optimal azimuth line of sight scan angle of 47 degrees, of about 3–23%, depending upon elevation scan angle and channel position on the array detector. This has presented major challenges to the data analysis methods and implementation. An extended and intensive effort was made to characterize the radiative properties of the obstruction and to correct measured radiances accordingly [*Gille et al.*, 2008, 2005]. The key challenge has been to accurately model the time-variant thermal characteristics of this obstruction, on multiple timescales, ranging from the subprofile level, through the interorbit level, to annual variability dominated by change in the orbital minimum angle between sun and zenith. The HIRDLS ozone profiles discussed in this article are retrieved from these corrected radiances with the current version processors: v2.04.09 [*Gille et al.*, 2008].

[4] The original HIRDLS observation mode was intended to take vertical limb scans at multiple azimuth locations behind AURA, thereby giving multiple parallel zonally staggered measurement curtains following AURA, approximately separated by 500 km. Owing to the presence of the optical obstruction a single near-limit azimuth angle of −47 degrees (starboard, or to the right) is used to repeatedly scan in an up-down elevation cycle. The azimuth indicated presents the optimum combination of predictability and large open area fraction (unobstructed percentage of the cross section of the optical path). All measurements presented here are taken at this azimuth angle.

[5] The various comparisons presented here are taken from a pool of about 490 days completed with the v2.04.09 processor as of September 2007, about half of which were selected to maximize the coincidence with the various correlative validation measurements taken by or on various platforms and on various validation campaigns.

[6] HIRDLS ozone is compared with ozonesondes, including from the Southern Hemisphere Additional Ozonesonde (SHADOZ) network and the Sodankylä Total Ozone Intercomparison and Validation (SAUNA) and Water Vapor Validation–Satellite/Sondes (WAVES) campaigns, with ground-based lidar systems (Table Mountain Facility (TMF), Mauna Loa Observatory (MLO) and Observatoire de Haute Provence (OHP)), airborne lidar (GSFC-AROTAL) and with satellite measurements (Atmospheric Chemistry Experiment Fourier Transform Spectrometer (ACE-FTS), Microwave Limb Sounder (MLS)).

2. Data Evaluation

[7] All comparisons shown in this paper will be on a pressure grid. HIRDLS pressure is determined in a joint retrieval with temperature (R. Khosravi et al., Retrieval Algorithm and Characterization of for the High Resolution Dynamics Limb Sounder, manuscript in preparation, 2008). There are as yet unresolved issues relating to the HIRDLS geopotential height calculation so altitude is not currently published in HIRDLS v2.04.09 public data files. References to altitude will be made only in regard to describing specifications, capabilities or errors associated with ozonesondes, lidars or other instruments. Reference to height made in the context of HIRDLS data or comparisons will be made in terms of pressure (i.e., greater height = lower pressure).

2.1. Filtering

[8] Two of the three HIRDLS ozone channels (10, 12) are especially sensitive to the presence of clouds, which manifest themselves as large spikes in the retrieved ozone, several orders of magnitude larger than realistic values, at heights generally earthward of about 50 hPa. Although clouds are detected in the standard HIRDLS v2.04.09 level 2 processing [*Massie et al.*, 2007; *Gille et al.*, 2008] and species retrievals, including ozone, are carried out only down to the cloud top level, spikes remain present in some ozone profiles that appear to be associated with the presence of clouds, especially equatorward of ±30° latitude.

[9] Since these cloud-like spike features tend to obscure other cloud-free and potentially good retrieved ozone values in the statistical difference evaluations, a postprocessor spike removal filter technique is implemented to remove ozone values where these large spikes are observed. This filtering consisted of determining the ozone vertical gradient, flagging the pressure level at which the gradient exceeds an empirically determined threshold value, and truncating the profile earthward of that level. Limitations of this technique manifest themselves as slight upturns in the earthward end of ozone profiles, when filtering is inadequate, or profiles that are truncated excessively at the earthward end. The effect due to over filtering is minimal, and the effect of under filtering is seen as residual positive HIRDLS ozone bias.

[10] The cloud-related spike filter is applied to HIRDLS ozone coincident with all sonde and lidar measurements, which are the main sources for low-latitude validation, where spikes are most prevalent. It is applied to the middle- and high-latitude cases for consistency but has a minimal effect there. Filtering also has a small effect on the comparisons with lidar, even at low latitudes, since these are almost by definition cloud free and hence nearly spike free. It should be noted that cloud-free conditions over a lidar station does not guarantee cloud free conditions for a coincident satellite limb measurement with a coincidence criterion of several hundred kilometers. This kind of filtering is only partially effective, and should become less relevant as cloud detection sensitivity and its implementation with respect to HIRDLS species retrievals

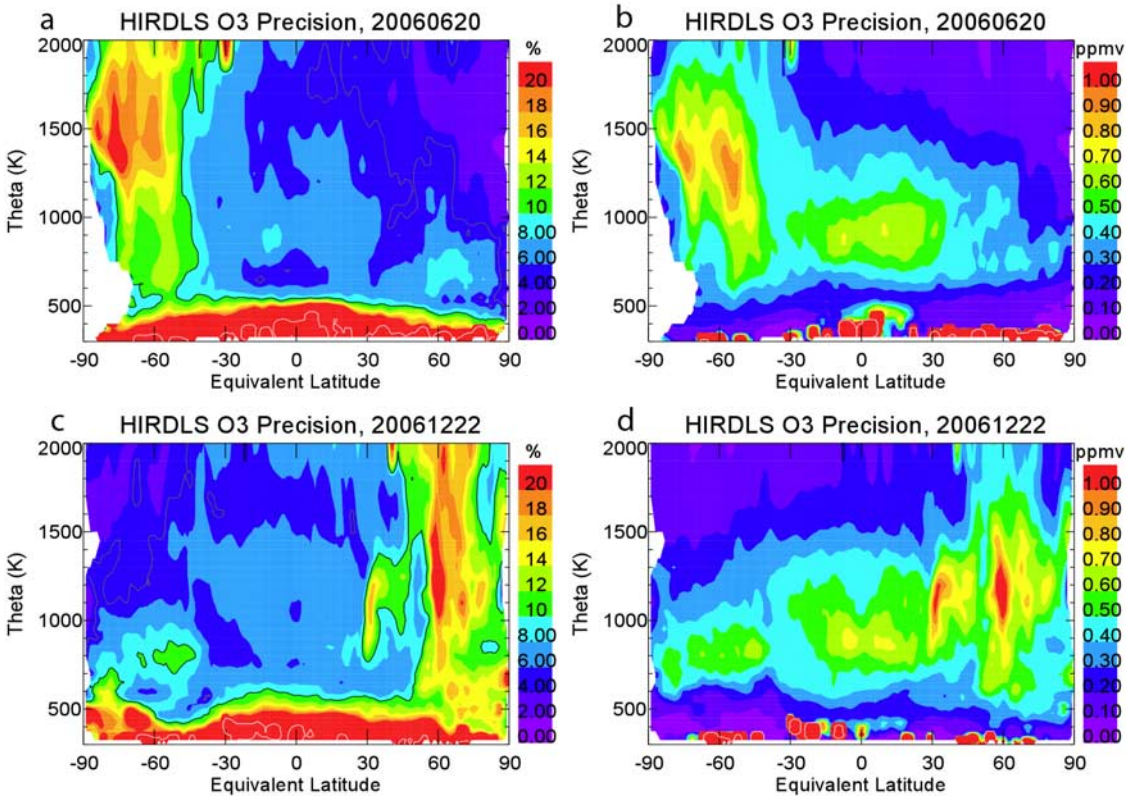

Figure 1. (a–d) Shown is the ozone standard deviation in different equivalent latitude and potential temperature bins, an estimate of High Resolution Dynamics Limb Sounder (HIRDLS) ozone precision. Results are given for 2 days, 20 June 2006 (Figures 1a and 1b) and 22 December 2006 (Figures 1c and 1d), in terms of both percentage of ozone mixing ratio (Figures 1a and 1c) and ozone mixing ratio directly (Figures 1b and 1d). In Figures 1a and 1c, the black lines highlight the 10% contour, and the white lines highlight the 100% contour.

is improved upon in cloud detection algorithms currently being developed.

[11] There is an additional filter that is implemented in all HIRDLS data shown here. HIRDLS data points are omitted in all cases where the level-2-retrieval total ozone error is negative. The total error is calculated by the optimal estimation retrieval algorithm, and is a combination of the a priori error, and the propagation errors of the radiance measurements (R. Khosravi et al., manuscript in preparation, 2008). A negative sign on the total error is an indicator that greater than 50% of the contribution to the error originates from the a priori input to the retrieval. This filtering minimizes the possibility that we use, and validate, ozone with the largest a priori influence.

2.2. Ozone Precision

[12] An estimate of HIRDLS ozone precision can be made on the basis of ozone variability in different bins, sorted horizontally by equivalent latitude and vertically by potential temperature, where geophysical variability is expected to be at a relative minimum. Twenty-four hour periods of HIRDLS data are interpolated onto a potential temperature grid, and then clustered into 4-degree equivalent latitude bins centered on 1-degree increments (essentially a 4-degree wide boxcar smoothing in latitude). The equivalent latitude is defined from Met Office potential vorticity data. The standard deviation for all measurements within equivalent latitude bins is calculated at each potential temperature level. An additional criterion is applied that limits the measurements to those that are within 5 degrees in geographic latitude of the average geographic latitude in the equivalent latitude bin. This is done to avoid variations due to substantially different amounts of solar insolation. Ozone values, where ozone error is greater than 30% of the actual ozone magnitude, are filtered to further prevent highly variable geophysical structure at winter high latitudes from translating into the equivalent latitude field; this has no significant effect elsewhere.

[13] Figure 1 shows standard deviation contours for two dates, chosen to represent Northern Hemisphere (NH) summer and Southern Hemisphere (SH) summer. Values for other days are similar, taking into account seasonal variations (i.e., more variations are seen during winter at high equivalent latitudes). These precision estimates indicate that ozone precision is approximately 5–10% between about 500 and 2000 K vertically (20–50 km, or ~1–50 hPa) at low latitudes and at summer hemisphere middle to high latitudes as well. At winter hemisphere high latitudes (poleward of 50°) the standard deviation degrades significantly, with the worst values as high as 20–30% at 1500 K (~42 km or ~2 hPa). These high standard deviation values (low precision estimates) may be less an indication of an

Table 1. SHADOZ Stations With Their Geographical Locations, Ozonesonde KI Cathode Sensing Solution Used, and Pump Manufacturer[a]

Station	Location	KI Cathode Solution	Pump
Ascension Island	7.98°S, 14.42°W	1% KI buffered	varies
Cotonou, Benin	6.21°N, 2.23°E	1% KI buffered	SPC 6A
Heredia, Costa Rica	10°N, 84.11°W	1% KI (1/10th) buffered	EnSci 2Z
Irene, South Africa	25.9°S, 28.22°E	1% KI buffered	SPC 6A
Kuala Lumpur, Malaysia	2.73°N, 101.7°E	1% KI buffered	SPC 6A
Malindi, Kenya	2.99°S, 40.19°E	1% KI buffered	SPC 6A
Nairobi, Kenya	1.27°S, 36.8°E	1% KI buffered	EnSci 2Z
Natal, Brazil	5.42°S, 35.38°W	1% KI buffered	EnSci Z, SPC 6A
Paramaribo, Surinam	5.81°N, 55.21°W	1% KI buffered	SPC 6A
Suva, Fiji	18.13°S, 178.4°E	2% KI unbuffered	SPC 6A
Watukosek (Java), Indonesia	7.5°S, 112.6°E	2% KI unbuffered	EnSci 2Z
Pago Pago, American Samoa	14.23°S, 170.56°W	2% KI unbuffered	SPC 6A
San Cristóbal, Galapagos	0.92°S, 89.6°W	2% KI unbuffered	SPC 6A
Réunion Island	21.06°S, 55.48°E	0.5% KI buffered	EnSci Z, SPC 6A

[a]SHADOZ: Southern Hemisphere Additional Ozonesonde.

actual HIRDLS ozone precision, and more an indication that rebinning the data into equivalent latitude and potential temperature is less effective at producing the intended effect of separating out geophysical variability from the random variability, owing to the presence of highly variable ozone in the winter vortex. It should also be noted that one would expect a real reduction in HIRDLS accuracy, rather than precision, in regions of high spatial variability such as winter high latitudes, owing to some unavoidable degree of averaging that occurs over the line of sight of any limb-viewing instrument. R. Khosravi et al. (manuscript in preparation, 2008) discuss the averaging kernels associated with HIRDLS measurements.

3. Ozonesondes

[14] Comparisons with several ozonesonde data sets are reviewed here from (1) the low-latitude Southern Hemisphere Additional Ozonesonde (SHADOZ) network, (2) the high-latitude Sodankylä Total Ozone Intercomparison and Validation (SAUNA) campaign in Sodankylä, Finland (67.4°N), during spring 2006, and (3) the midlatitude Water Vapor Validation–Satellite/Sondes (WAVES) campaign in Beltsville, Maryland (39°N), during summer 2006.

[15] There is a certain amount of variability associated with use of ozonesondes, as each sonde is a unique instrument, especially when station-dependent factors are considered [*Thompson et al.*, 2003a, 2003b, 2007; *Liu et al.*, 2006; *Logan et al.*, 1999]. Among the conditions that factor into this variability are (1) the manufacturer of the instrument used (ENSCI-Corporation sondes can read 5–10% higher than sondes from Science Pump Corporation (SPC), above 20 km [*Thompson et al.*, 2007; *Smit et al.*, 2007]); (2) the concentration of potassium iodide (KI) sensing cathode solution used, and whether or not it includes a buffering agent may also produce variances of 15% above the partial pressure layer peak [*Johnson et al.*, 2002]; and (3) whether and how pump efficiency correction factors are implemented, which may also cause differences of up to 15% at upper altitudes [*Johnson et al.*, 2002].

[16] The 1% buffered solution has been the historical standard and is still the most commonly used within the SHADOZ network. The 0.5% KI buffered cathode solution is currently recommended by ENSCI Corporation. It is now in use at multiple sites within the Network for the Detection of Atmospheric Composition Change (NDACC, formerly NDSC), which is dedicated, among other things, to the long-term measurement and monitoring of atmospheric composition and structure. The 0.5% KI buffered cathode solution was used exclusively during the SAUNA and WAVES campaigns.

[17] Generally, it can be said that the precision for ozonesondes is about 5% [*Barnes et al.*, 1985; *Johnson et al.*, 1998, 2002; *Thompson et al.*, 2003a]. Agreement of SHADOZ ozone with independent measurements is 5%, with systematic station-dependant biases [*Thompson et al.*, 2003a]. More recent comparisons of the total column with TOMS (version 7) agree to within 2–4% [*Thompson et al.*, 2007]. Within the SHADOZ network there is significant variability in tropospheric ozone, with deviations of 50% relative to the Pacific mean that are likely of geophysical origin, and some variability in stratospheric ozone, less than 10% relative to the Pacific mean, that may be partially geophysical and partially due to station-dependant instrument bias [*Thompson et al.*, 2007].

3.1. SHADOZ Network

[18] The SHADOZ ozonesonde network currently consists of fourteen stations located in the tropics, approximately within $-26°S < \text{latitude} < 10°N$ [*Thompson et al.*, 2003a, 2003b, 2007]. It should be noted that the different stations use the three most common variations of the KI cathode sensing solution. The station locations, KI cathode solution, and pump manufacturer used at each station are summarized in Table 1. Nine of the stations use the 1% KI buffered solution, four stations use the 2% KI unbuffered solution and a single station uses the 0.5% KI buffered cathode solution. Each station used consistently the indicated concentration during the entire period of this validation study. Different sites used KI solution types in combinations with different pumps, sometimes contrary to manufacturer recommendation, which can be expected to have effects nearly as strong as those introduced by the solution recipe itself. The combination of 2% solution with the Science Pump (SPC) sondes will generally produce the lowest ozone readings [*Thompson et al.*, 2007]. The 1/10th

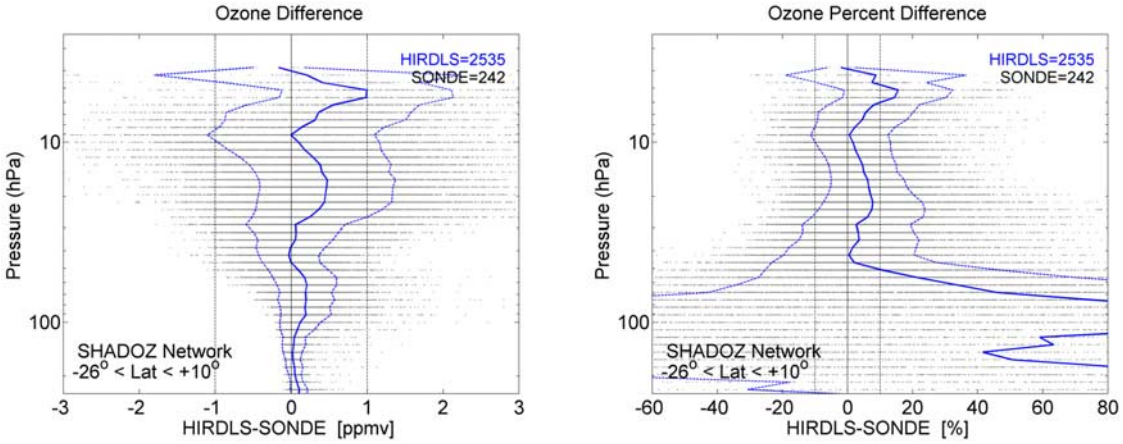

Figure 2. Shown are ozone differences between HIRDLS and 244 ozonesondes from the Southern Hemisphere Additional Ozonesonde (SHADOZ) network (26°S to 10°N, with a wide longitudinal distribution). Ozone differences are shown in terms of (left) mixing ratio and (right) percent of sonde values. The mean differences are the solid blue lines, the standard deviations are the dashed blue lines bracketing the mean, and the individual differences from which these are derived are the horizontally distributed layers of black dots (visible as gray lines of varying intensity). All differences here are HIRDLS minus ozonesonde, so negative differences denote low HIRDLS values. This format is used in all similar plots in this paper.

normal buffer strength used with the 1% KI solution in the Heredia station, will yield performance more like that of the 2% unbuffered solution [*Johnson et al.*, 2002].

[19] The temporal and spatial criteria used to determine coincidence are: HIRDLS profiles must be within 12 hours and within 560 km (circle with 5 degree latitude radius) of the sonde launch time and launch site, respectively. About 240 SHADOZ sondes match the coincidence criteria for the 490 HIRDLS dates available. Typically there are 6 to 20 coincident HIRDLS profiles for any given ozonesonde. The ozone difference is calculated for each HIRDLS-ozonesonde profiles pair that matched these criteria for all SHADOZ sites. Individual profile comparisons are presented in section 2.4. The ozonesondes in this data set reached burst pressures as low as 4 hPa (~37 km).

[20] The mean and standard deviation of all ozone-difference profiles are shown in Figure 2 in terms of volume mixing ratio (ppmv) and in terms of percentage (of ozonesonde values). The mean difference is within 10% between 6 hPa and 50 hPa, and is often 5% or better. At heights above 6 hPa the mean difference reached 15%. At 50 hPa the magnitude of the difference increased rapidly with increasing pressure, reaching a difference of about 50% at about 70 hPa. This is probably a result of the smaller cloud-related spikes that passed through the postprocessor filtering. This algorithm may soon become unnecessary as improvements to the current operational cloud detection algorithm are implemented.

3.2. SAUNA Campaign

[21] SAUNA was a high-latitude campaign, based in Sodankylä, Finland, which took place from mid-March to early May 2006. The 0.5% KI cathode solution concentration was used with all SAUNA ozonesondes shown here. Sondes in this data set also reached burst pressures of about 4 hPa (~36 km). Differences are computed in the same way as was done for the SHADOZ sondes, and are shown in Figure 3. The mean difference at pressures between 7 and 30 hPa is generally better than 10%. At heights above 7 hPa the difference increases to slightly more than 10%, similar to what was found for SHADOZ sondes. Between 30 and 70 hPa, the mean difference is between negative 10 and 15%. At 70 hPa the magnitude of the difference increases rapidly with increasing pressure, reaching a difference of about 50% at about 200 hPa, in a pattern similar to what is seen in many of the other HIRDLS correlative data comparisons.

3.3. WAVES Campaign

[22] WAVES was a midlatitude campaign, based in Beltsville, Maryland, which took place during July and August of 2006. The maximum sonde height among the coincident sondes shown here was 9 hPa (32 km). Excellent coincidence was achieved, typically between 15 to 150 minutes temporally and frequently less than 150 km spatially.

[23] The resulting mean difference (Figure 4) is slightly better than what was found with SAUNA, with generally less than 5% difference between 40 hPa and 9 hPa, and with a reduced range, 50–70 hPa, over which the mean difference is between negative 10 and 15%. Here again, at 70 hPa the magnitude of the difference increased rapidly with increasing pressure, reaching a difference of about 50% at about 150 hPa. This decisive degradation with increasing pressure (decreasing height), which begins somewhere between about 50 and 100 hPa, depending on latitude, is a feature which is present for all of the sonde comparisons just shown, as well as for other comparisons to be shown here. This may be caused by unfiltered cloud-related spikes, which may be expected to occur at greater pressures with increasing latitude.

3.4. Ozonesonde Profile Comparisons

[24] Looking at ozone differences from the statistical point of view, as was just done, does not allow for

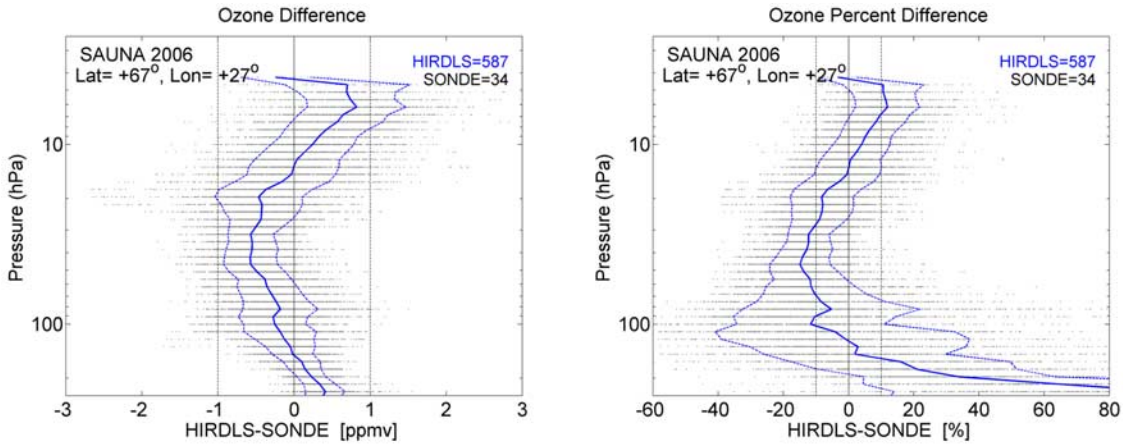

Figure 3. Shown are mean (solid blue) and the standard deviation (dashed blue) of the ozone differences between HIRDLS and ozonesondes (34 sondes using 0.5% KI cathode solution) from the spring 2006 Sodankylä Total Ozone Intercomparison and Validation (SAUNA) campaign carried out at Sodankylä, Finland (67°N, 27°E).

evaluation of the vertical resolution of HIRDLS ozone measurements. In order to do so, a more detailed look at individual sonde comparisons with coincident HIRDLS profiles is useful. If the small vertical-scale features that are routinely exhibited in the HIRDLS measurements are real, one would expect to see similar features, at least some of the time, in the sonde profiles, as sondes clearly have the benefit of high vertical resolution.

[25] One would not expect to always see similar fine vertical-scale features in both sonde and HIRDLS profiles, even in a hypothetical case with very well matched coincidence criteria and where it was known beyond any doubt that HIRDLS had very high vertical resolution. The obvious reason for this is that the viewing geometries and the sampling timescales of the two platforms are inherently different. The in situ sonde sampling contrasted against the several hundred kilometer HIRDLS limb, as well as the 15 second HIRDLS profile compared to the 2 hour sonde profile, introduces some ambiguity to the precisely defined and measured coincidence criteria.

[26] Figure 5 is a 10-panel plot of individual sonde profiles compared with the series of coincident HIRDLS profiles that matched the coincidence criteria used in the statistical studies above. Figures 5a–5f are taken from various SHADOZ sites, and Figures 5g–5j are from the SAUNA and WAVES campaigns. It is fairly obvious that many of the fine vertical features seen in the sonde profiles are also seen in the HIRDLS profiles. This is most clearly seen in subplots (Figure 5a) and (Figure 5b) from La Reunion Island. Here, fine-scale features are mirrored over nearly the full range of overlap of the sonde and HIRDLS profiles. One can see the agreement in the more obvious features near 10–20 hPa, but also in the more subtle features present in the underside of the ozone layer near 50 hPa. These are also exhibited to varying degrees in SHADOZ profiles (Figures 5c–5e) and WAVES profiles

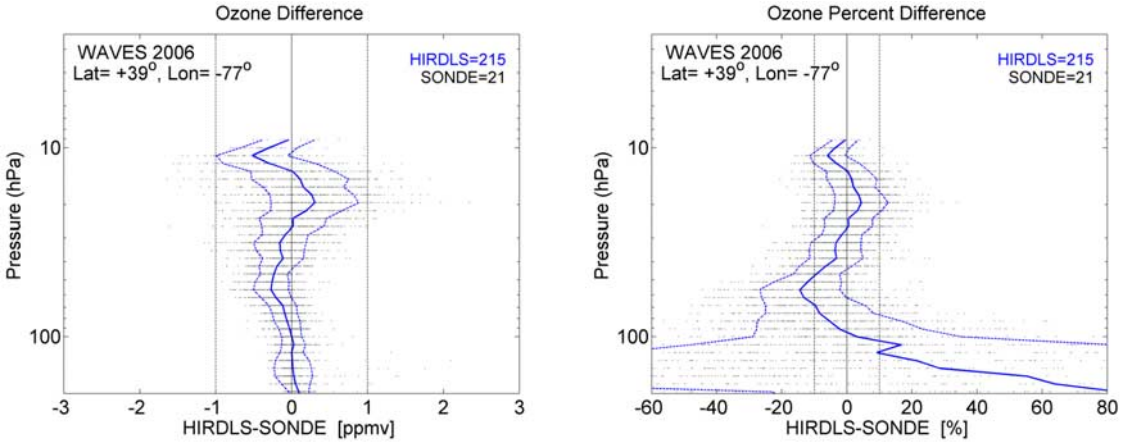

Figure 4. Shown are mean (solid blue) and the standard deviation (dashed blue) of the ozone differences between HIRDLS and ozonesondes (21 sondes using 0.5% KI cathode solution) from the summer 2006 Water Vapor Validation–Satellite/Sondes (WAVES) campaign carried out in Beltsville, Maryland, 39°N, 77°W.

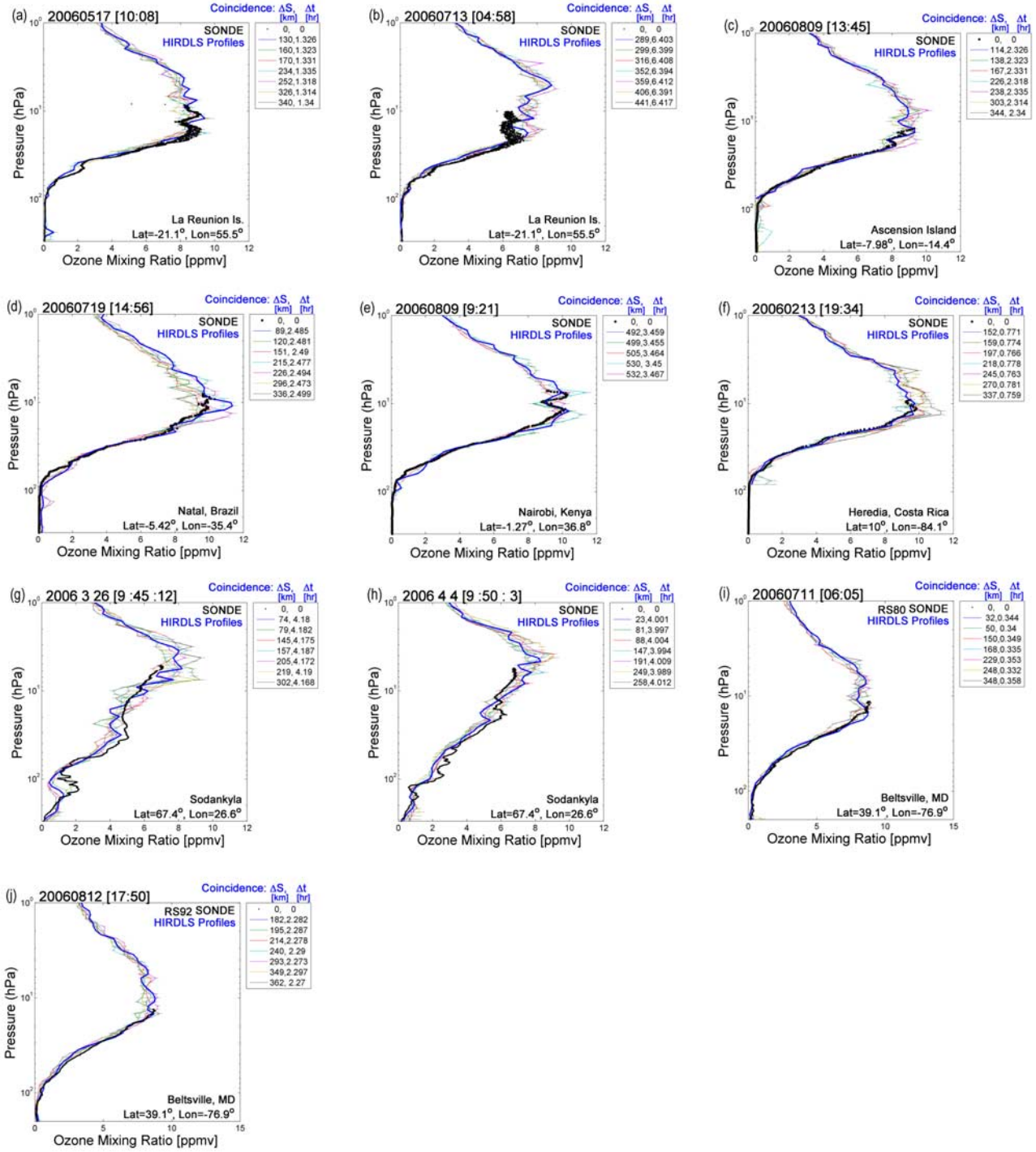

Figure 5. Individual ozonesonde profiles are compared with the nearest HIRDLS profiles: (a–f) SHADOZ, (g, h) SAUNA, and (i, j) WAVES. Ozonesonde profiles are represented by black dots; the coincident HIRDLS profiles are the colored lines. The legend contains two numbers separated by a comma: the first denotes the geophysical separation of the HIRDLS profile from the sonde in kilometers, and the second denotes the separation in hours. The closest of the coincident HIRDLS profiles is the bold blue line in the plot. South latitudes and west longitudes are denoted as negative in the labels.

(Figures 5i and 5j). The Heredia profile (Figure 5f) appears to reproduce the subtle contour throughout the profile leading up to the sharp peak at 15 hPa. This may be coincidence, but it is not unusual.

[27] The high-latitude SAUNA profiles (Figures 5g and 5h) showed the greatest disparity in terms of both fine-scale structure and magnitude. Though larger-scale features seemed to be captured and some small-scale features seem

to be present in both measurements, it is more difficult to conclude that HIRDLS is capturing the fine-scale variability.

[28] A likely cause for this relates to limitations in actual coincidence alluded to earlier. The 2006 Arctic late winter/early spring was a very dynamic period which experienced a strong stratospheric sudden warming causing a breakup of the polar vortex, followed by a strong reformation of the vortex in the upper stratosphere [*Randall et al.*, 2006; *Manney et al.*, 2007]. Under these circumstances you expect to have extremely variable ozone both vertically and horizontally, as relatively low-ozone vortex air mixes with higher ozone air previously outside the vortex in varying degrees with height. This accentuates coincident-observation ozone discrepancies caused by differences in sampling domains of the different instruments. It represents an extreme case and a limitation for HIRDLS or any other limb-viewing instrument.

4. Ground-Based Lidar

[29] HIRDLS ozone was compared to three differential absorption lidars (DIAL) operated under the NDACC network. These lidar systems are located at (1) the Mauna Loa Observatory, Hawaii (MLO) (19.5°N, 155.6°W), (2) the Table Mountain Facility, California (TMF) (34.4°N, 117.7°W), both operated by the Jet Propulsion Laboratory (JPL), and (3) the Observatoire de Haute-Provence, France (OHP) (43.9°N, 5.71°E) operated by the Centre National de la Recherche Scientifique (CNRS).

[30] Details of the implementation of the DIAL method for measuring stratospheric ozone are described for OHP by *Godin et al.* [1989], for TMF by *McDermid et al.* [1990], and for MLO by *McDermid et al.* [1995]. The full measurement ranges of these lidars are as follows: TMF, 4–55 km; MLO, 15–55 km; and OHP, 10–45 km. Each of these lidars routinely performs nighttime measurements averaged over several hours, about three nights per week on average.

[31] In the case of MLO and TMF the ozone total uncertainty (including both precision and accuracy) ranges from 2% at the center of the ozone number density peak (22–25 km) to 50% and more below 14 km (owing to the rarity of ozone) and above 45 km (owing to the drop of signal-to-noise ratio). The OHP total accuracy also ranges from a few percent below 20 km to greater than 10% above 45 km [*Godin-Beekmann et al.*, 2003] and has horizontal spatial resolution of about 100 km. In all three lidars the vertical resolution varies with altitude, ranging from several hundred meters in the lower part of the profiles to about 2 to 8 km at the top of the profiles.

[32] At MLO and OHP two additional wavelengths are detected in order to retrieve ozone in case of high aerosol loading [*McGee et al.*, 1993]. Under normal conditions the TMF also has this capability, but it was not operational during this Aura validation period owing to maintenance issues. TMF also operates an additional Rayleigh lidar system for tropospheric ozone measurements (4–25 km) since 1999 [*McDermid et al.*, 2002]. The vertical resolution of these profiles runs from 75 m in the lower troposphere to 4–5 km in the lower stratosphere. The ozone total uncertainty ranges from 5% at the bottom of the profile to 15% at the top.

[33] The pressure profile, which is the grid used to compare with HIRDLS ozone, is determined by normalizing the lower altitude Raman channel, if available, to the closest-in-time radio sounding(s). If two soundings were made within 12 hours of the lidar measurements, both are used (time interpolation). When a local radiosonde is not available, the source is NCEP 12Z available though NDACC (normalized at 30+ km). The upper lidar channels are simply normalized to the lower ones after the latter have been normalized to NCEP or radiosonde [*Leblanc et al.*, 1998].

4.1. Comparisons: MLO, TMF, and OHP

[34] The same temporal and spatial coincidence criteria are used for the lidars as were used for ozonesonde comparisons, namely, 12 hours and a 560 km radius. The same comparisons are also done with lidar measurements as were done with ozonesondes: a statistical difference analysis to quantify systematic bias; and examination of individual profile comparisons to gain a better understanding of the HIRDLS vertical resolution capability.

[35] Although lidars give localized, high vertical resolution profiles, much as ozonesondes do, there are several noteworthy differences that may have an effect on comparisons with HIRDLS. The most obvious difference is that these lidars have a vertical range that extends up to 20 km higher into the stratosphere than the sondes, allowing for comparisons of the top side of the ozone layer (in VMR). A less obvious difference is that although they are both roughly 2 hour measurements, the lidar profile is a time integrated measurement over the full range of the profile, whereas the sonde is a sliding snapshot with a height-time dependency. The result is that one should expect a certain amount of smoothing to effectively occur in the lidar profiles, due to averaging of any short-timescale vertically dependent variability, if and when present.

[36] Figures 6, 7, and 8 show the mean and standard deviation of the difference profiles between HIRDLS and lidar, for MLO, TMF and OHP, respectively. In general, HIRDLS ozone compared slightly better with MLO and TMF than it did with OHP. Agreement with MLO and TMF was within 5% between 2 and 40 hPa, with the exception that between 12 and 25 hPa HIRDLS ozone was 5–10% high compared to MLO. Compared with OHP, HIRDLS ozone was generally within 10% between 2 and 40 hPa, with the exception that between 5 and 10 hPa HIRDLS was slightly more than 10% higher. One can also see clearly that the HIRDLS bias is fairly consistently high between 5–20 hPa in comparison with all three lidars.

[37] At roughly 50 hPa HIRDLS ozone tends to be 10–15% low compared with all three lidars. With increasing pressure beyond 50 hPa, the difference becomes rapidly more positive as the standard deviation also increases rapidly. This behavior is very similar to what is observed in the ozonesonde comparisons, especially for SAUNA and WAVES, and may have the same root cause. At pressures less than 2 hPa comparisons are more erratic as the standard deviation of the difference becomes rapidly larger; this coincides with the upper height range of useful lidar measurements as established in their specifications.

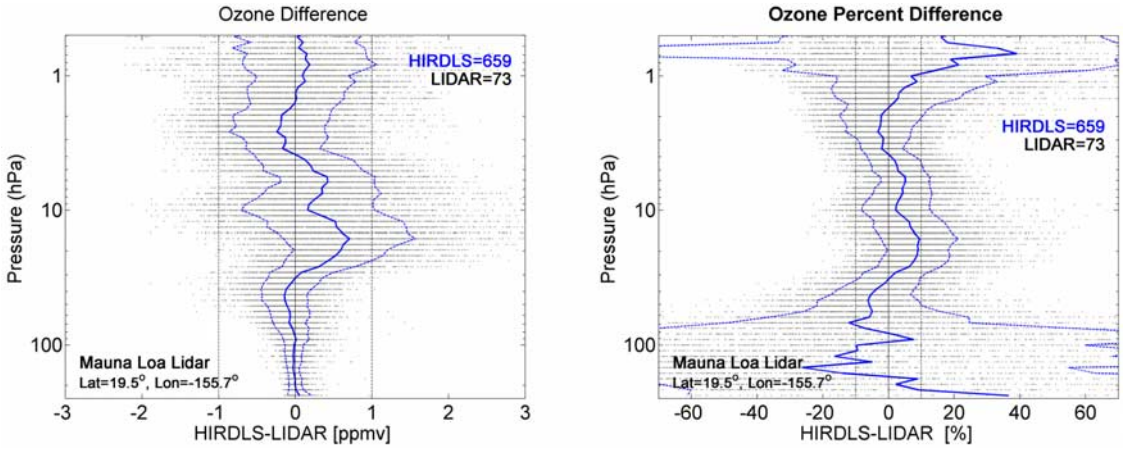

Figure 6. Shown are ozone differences between 73 Mauna Loa Observatory (MLO) lidar profiles and the 659 coincident HIRDLS profiles, in terms of (left) mixing ratio and (right) percent of lidar values. The mean differences are the solid blue lines, the standard deviations are the dashed blue lines bracketing the mean, and the individual differences from which these are derived are the horizontally distributed layers of black dots (visible as gray lines of varying intensity).

4.2. Lidar Profile Comparisons

[38] Figure 9 shows individual profile comparisons with the MLO, TMF, and OHP lidars. Profile comparisons here echo the ozonesonde profile comparisons shown earlier. Many of the finest vertical features observed by lidar at all three stations are also visible in the coincident HIRDLS profiles. This appears to be true over nearly the full overlapping range of the profiles, up to the uppermost vertical regions where ozonesondes make measurements (pressures of 4 hPa), as indicated by Figures 9c and 9d. Some of the observed fine vertical features appear more pronounced in the HIRDLS profiles than they do in the coincident lidar profile (Figures 9a, 9c, and 9e). This is what one might expect to see in a scenario where there is relatively high temporal variability in a highly vertically structured ozone field. This structure would be smoothed in the 2 hour integration period over which the lidar profile is averaged, but would be captured in the ~15 second HIRDLS profiles if HIRDLS is indeed capable of resolving this vertical scale. In such a case one might also expect to see high variability between adjacent HIRDLS profiles, which appears to be the case at least in Figures 9a and 9e.

5. Airborne Lidar During INTEX-B

[39] During the Intercontinental Chemical Transport Experiment–B (INTEX-B) campaign in spring 2006, the AROTAL airborne lidar on board a DC-8 took nearly continuous measurements between latitudes 19°N and 58°N on 1 May 2006, between about 0745 UT and 1345 UT during the transition flight between Hilo, Hawaii, and Anchorage, Alaska. The path of the flight was directly under the HIRDLS measurement tract, which at these latitudes was fairly parallel to a meridian, roughly 151°W ± 1°. During this time, about 560 lidar profiles were taken all within 33 km, on average, from the nearest HIRDLS profile from among the 48 profiles coincident with the flight path. The obvious advantage here is proximity over a wide latitude range.

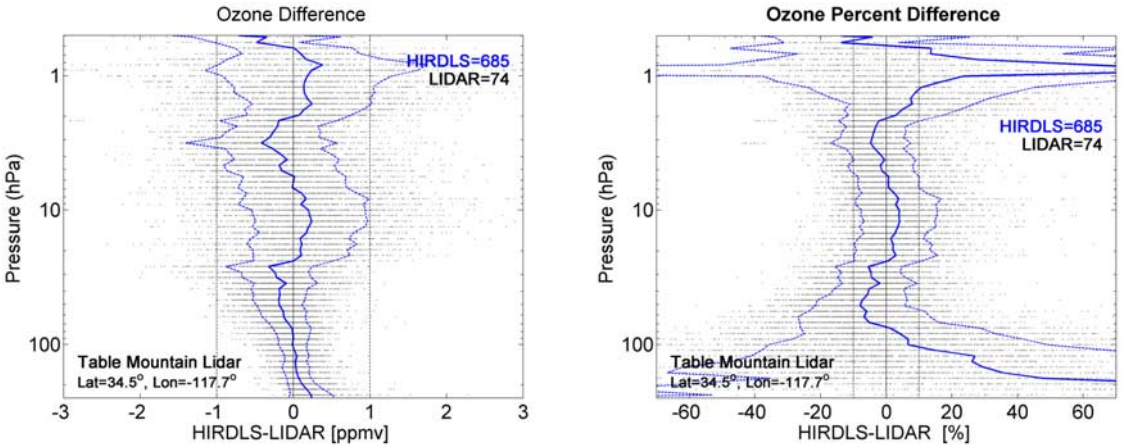

Figure 7. Shown are ozone differences between 74 Table Mountain Facility (TMF) lidar profiles and the 685 coincident HIRDLS profiles. The plot layout is the same as that in Figure 6.

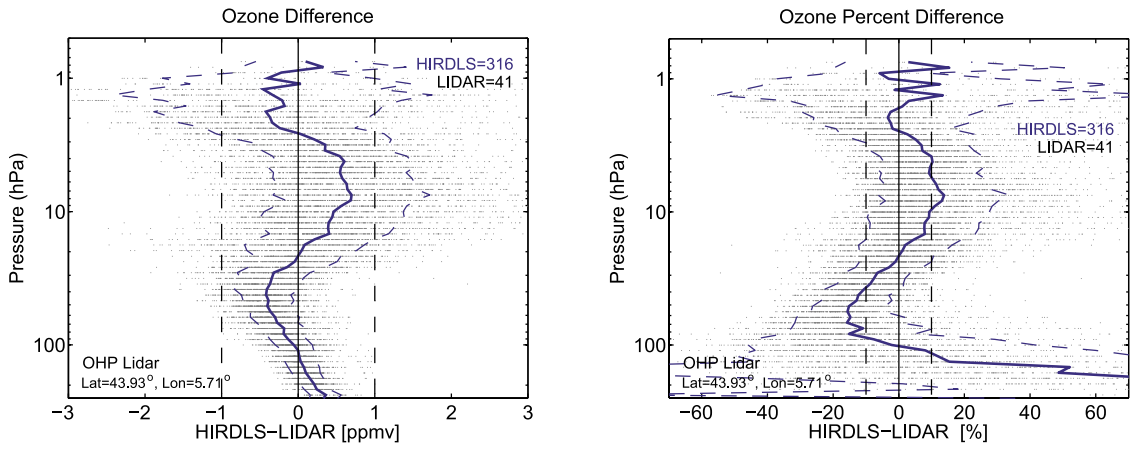

Figure 8. Shown are ozone differences between 41 Observatoire de Haute Provence (OHP) lidar profiles and the 316 coincident HIRDLS profiles. The plot layout is the same as that in Figure 6.

[40] The Airborne Raman Ozone Temperature and Aerosol (AROTAL) instrument combines a classic differential absorption lidar (DIAL) with a Rayleigh lidar and a Raman lidar, similar to the ground-based lidars described earlier. It is also capable of detecting ozone in case of high aerosol loading [*McGee et al.*, 1993], and has special optics and detectors that enable it to make ozone measurements in the presence of near-field cirrus clouds, during low-altitude dive maneuvers at night and in daylight, and down to the skin of the aircraft.

[41] AROTAL lidar profiles are stored on an altitude grid and are interpolated here onto a pressure grid using National Centers for Environmental Prediction (NCEP) model pressure, altitude, and temperature profiles produced for NDACC stations and available on the NDACC website. The pressure-altitude relationship at the latitude of each AROTAL profile is determined via interpolation between the nearest two NCEP profiles spanning it (in latitude) that are available in the NDACC database. This is then used to interpolate the AROTAL altitude-based profile onto the Aura pressure grid. A two-part comparison was then carried out between HIRDLS and AROTAL ozone profiles.

[42] First, the AROTAL transition-flight data set can be divided naturally into seven near-contiguous multiprofile segments, each of which spans several degrees of latitude, with between 43 to 96 profiles per segment (Figure 10, left). The coincident HIRDLS segments consist of series of three to six consecutive profiles per segment. The profiles for each instrument is averaged separately for each segment and plotted for comparison in Figure 10 (right). The region of overlap between averaged coincident profiles is between 8 and 100 hPa. The nature of this comparison removes by averaging any fine-scale vertical structure that may be present. However, one can see that HIRDLS and AROTAL profiles agree very well with regard to large-scale features and ozone magnitude. Slightly more structure is seen in the averaged HIRDLS profiles, but this is to be expected purely on the basis of the smaller number of profiles and the shorter time period over which HIRDLS measurements are averaged.

[43] In a second comparison, the statistical difference for all profiles was calculated. Each lidar profile was paired with the nearest HIRDLS profile and the difference profile was calculated. The average distance between all HIRDLS AROTAL profile pairs was 33 km. The resulting mean and standard deviation of all of the ozone difference profiles is shown in Figure 11, in terms of volume mixing ratio (ppmv) and percentage (of AROTAL values).

[44] Between 40 and 100 hPa HIRDLS ozone is well within 10% of AROTAL values, HIRDLS being consistently lower. Between 8 and 40 hPa HIRDLS ozone is within 5% of AROTAL values, generally low, but with an exception at about 30 hPa where HIRDLS ozone is several percent higher than AROTAL. Starting at about 60 hPa HIRDLS ozone bias steadily increases to a maximum of about positive 20% at about 150 hPa. This pattern is consistent with what was found in comparisons with sondes and ground-based lidars, and these results in general are very similar to those from comparisons with sondes and ground-based lidars.

6. Satellite Correlative Measurements

6.1. ACE-FTS

[45] HIRDLS profiles are compared here to coincident measurements from the Atmospheric Chemistry Experiment Fourier Transform Spectrometer (ACE-FTS) [*Bernath et al.*, 2005; *Walker et al.*, 2005; *Kerzenmacher et al.*, 2005; *Folkins et al.*, 2006]. ACE-FTS ozone profiles correspond to version 2.2 ozone. All ACE-FTS data were eliminated from the comparisons if there was a significant contribution from the a priori in the retrievals, but no other screening was performed on the ACE-FTS data.

[46] HIRDLS data poleward of 63°S were omitted from the comparisons because they were highly unrepresentative of the majority of the ACE Southern Hemisphere comparisons. The cause probably stems at least in part from issues related to an unfavorable limb-viewing geometry over regions of strong horizontal gradients near the winter polar vortex edge. Another possibly more important contributing factor may be that those profiles are taken when the spacecraft experiences local sunrise (crosses the terminator from night to day), producing a rapid temporal temperature gradient of the obstruction, which may not yet be predicted with adequate fidelity in the radiance correction scheme.

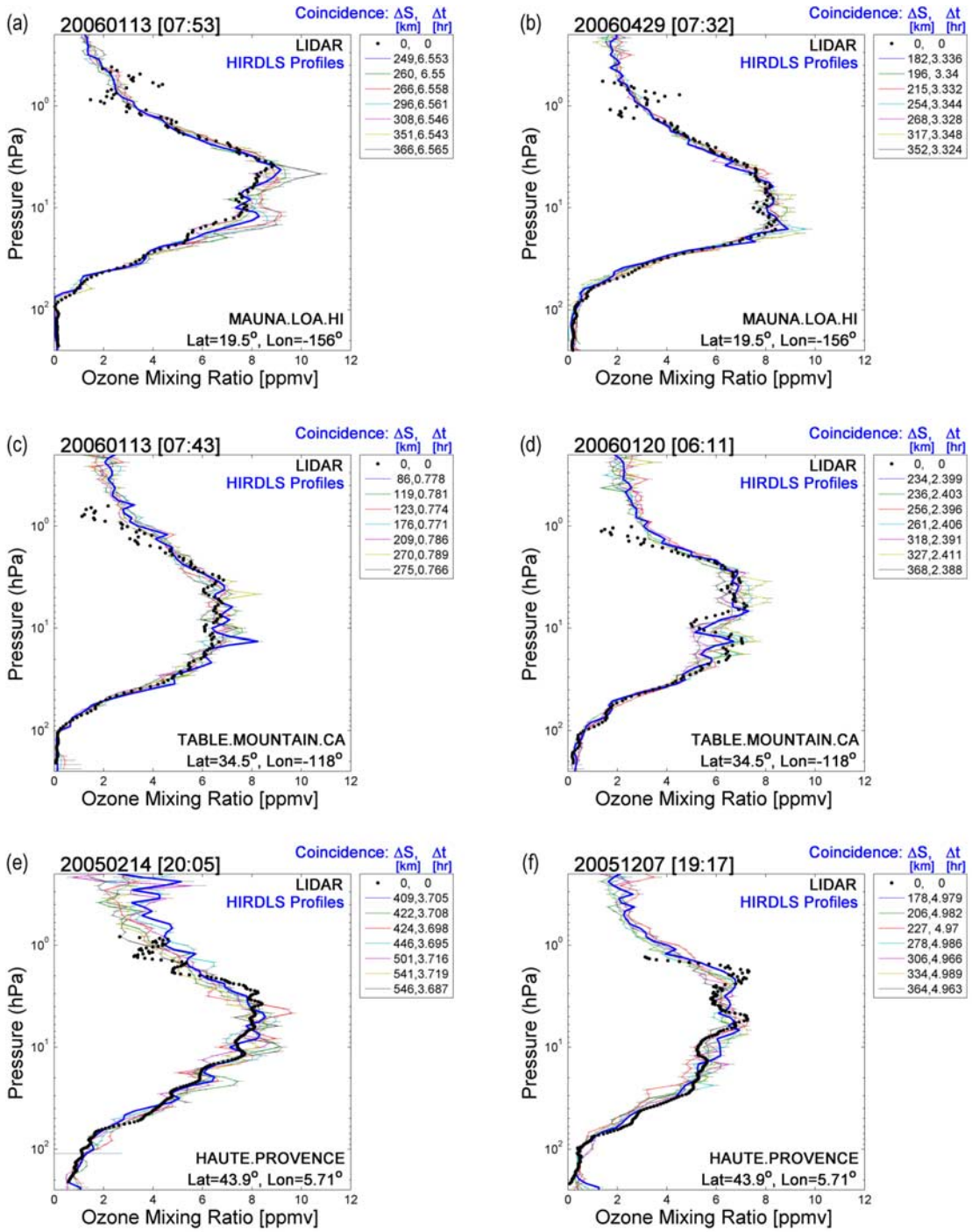

Figure 9. Comparisons of HIRDLS profiles with lidar profiles from (a, b) MLO, (c, d) TMF, and (e, f) OHP. Lidar profiles are represented by black dots; the coincident HIRDLS profiles are the colored lines, the closest being bold blue in the plot. The plot layout is the same as that in Figure 5.

[47] Coincidences were defined as occurring within 2 hours and 500 km, in the period extending from 18 May 2006 through 28 October 2006. A total of 225 ACE-FTS profiles on 24 different days were found to be coincident with at least one HIRDLS profile. There were often numerous HIRDLS profiles coincident with a single ACE-FTS profile. When this occurred, all of the coincident HIRDLS profiles were averaged together, and this average profile was compared to the ACE-FTS profile. Since the coincidences occur primarily at high latitudes, in the Northern Hemisphere (NH, 151 coincidences) or the Southern Hemisphere (SH, 74 coincidences), the two regions are compared separately.

[48] Comparisons of the mean profiles and the mean difference profiles for both hemispheres are shown in Figure 12. The average profiles and standard deviations of the distribution of profiles for both ACE and HIRDLS are shown in Figures 12a and 12b. A clear low bias in HIRDLS

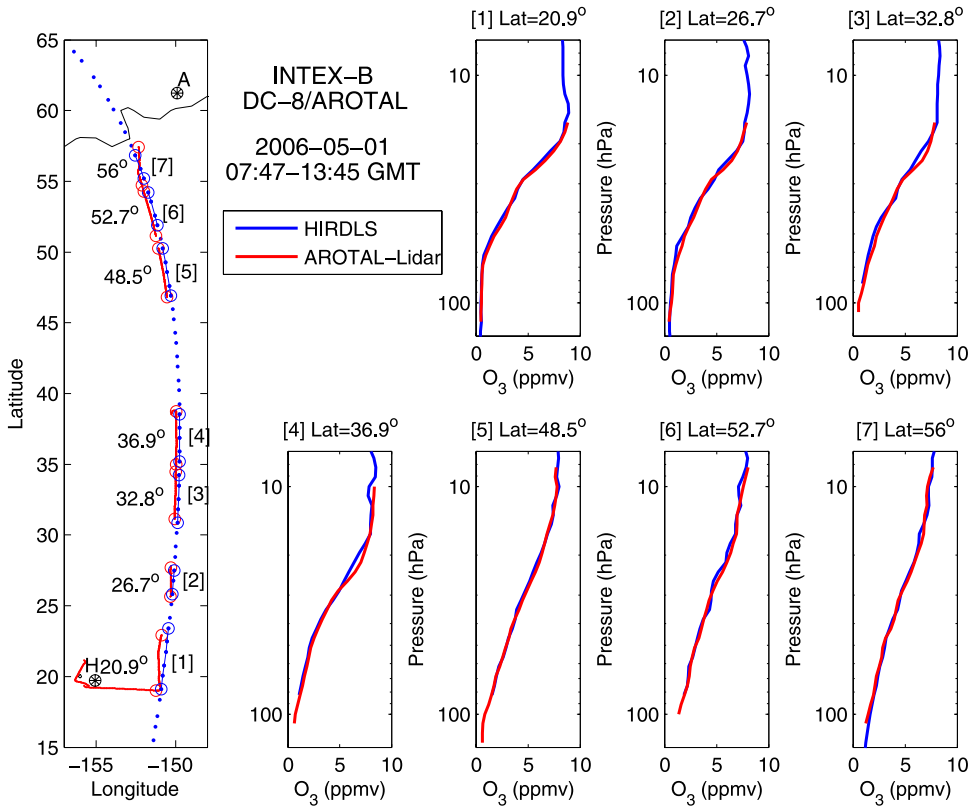

Figure 10. Shown is a comparison of HIRDLS ozone with Airborne Raman Ozone Temperature and Aerosol (AROTAL) differential absorption lidar (DIAL) during Intercontinental Chemical Transport Experiment-B (INTEX-B) transition flight on 1 May 2006, 0747–1345 UT, from Hilo, Hawaii (H) to Anchorage, Alaska (A). The leftmost plot shows the AROTAL (red) and HIRDLS (blue) measurement locations. The segment endpoints are denoted by circles, and segments are numbered in the square brackets. The averaged profiles for each of the seven segments are compared in separate plots at right (HIRDLS, blue; AROTAL, red), with titles indicating segment number and average segment latitude.

ozone can be seen through most of the vertical range, especially in the NH. Note that in SH the large standard deviation is due to a bifurcation of profiles from two distinctly different sets of coincidences: a set that occurred at latitudes of ~55–60°S in late May, and a set that occurred at latitudes of ~40–50°S in early October. This bifurcation represents a change in geophysical conditions, which at 10 hPa correspond roughly to 4–5 ppmv (55–60°S) and 6–7 ppmv (40–50°S) ozone levels.

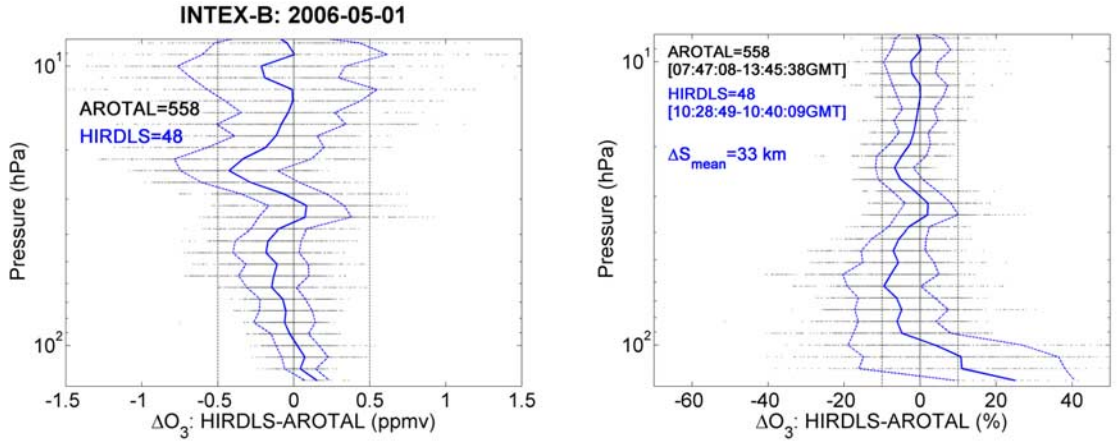

Figure 11. Statistical difference (HIRDLS–AROTAL) for all profiles compared. Each AROTAL profile is compared to the nearest HIRDLS profile. The mean coincidence distance between all profile pairs is 33 km.

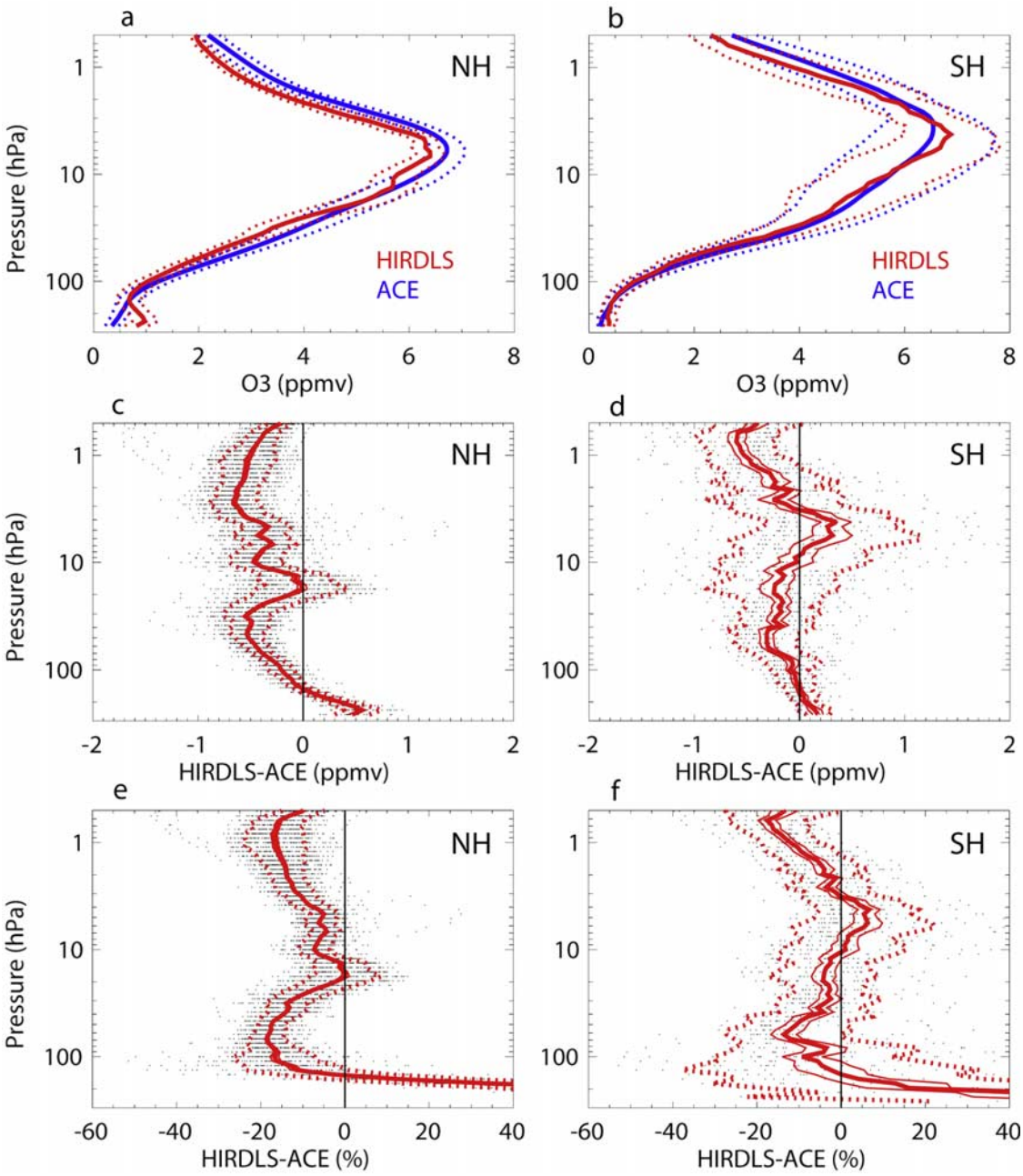

Figure 12. (a, b) The average and standard deviation of all the HIRDLS (red) and Atmospheric Chemistry Experiment Fourier Transform Spectrometer (ACE-FTS) (blue) ozone profiles. Figure 12a represents the Northern Hemisphere (NH), and Figure 12b represents the Southern Hemisphere (SH). The mean (solid red) and standard deviation (dashed red) of the difference (HIRDLS minus ACE-FTS) for all coincidences are shown in terms of (c, d) mixing ratio and (e, f) percentage. Negative numbers indicate low HIRDLS values. The individual differences from which these are derived are the horizontally distributed layers of small black dots. The thin red lines bracketing the mean, visible only in the SH, are the uncertainty in the mean (standard deviation divided by the square root of the number of points).

[49] Figures 12c–12f show the statistical differences between the coincident HIRDLS and ACE-FTS measurements, in terms of mixing ratio and percentage. The high-latitude SH ozone differences seem to be consistent with the northern high-latitude comparison using SAUNA ozonesondes, with a region where HIRDLS is low, between about 10 and 100 hPa peaking at negative 15–20%, and a region between about 5 and 10 hPa HIRDLS is up to 10% high. Though the ACE differences tend to show HIRDLS a bit lower than all other comparisons, especially in the NH, they are consistent with other comparisons in that HIRDLS tends to be generally low throughout the comparison range, but with a locally high spot somewhere in the middle of the range, between 5 and 30 hPa depending on the comparison. That the standard deviation of the ozone differences in the SH middle and lower stratosphere (10–100 hPa) is larger

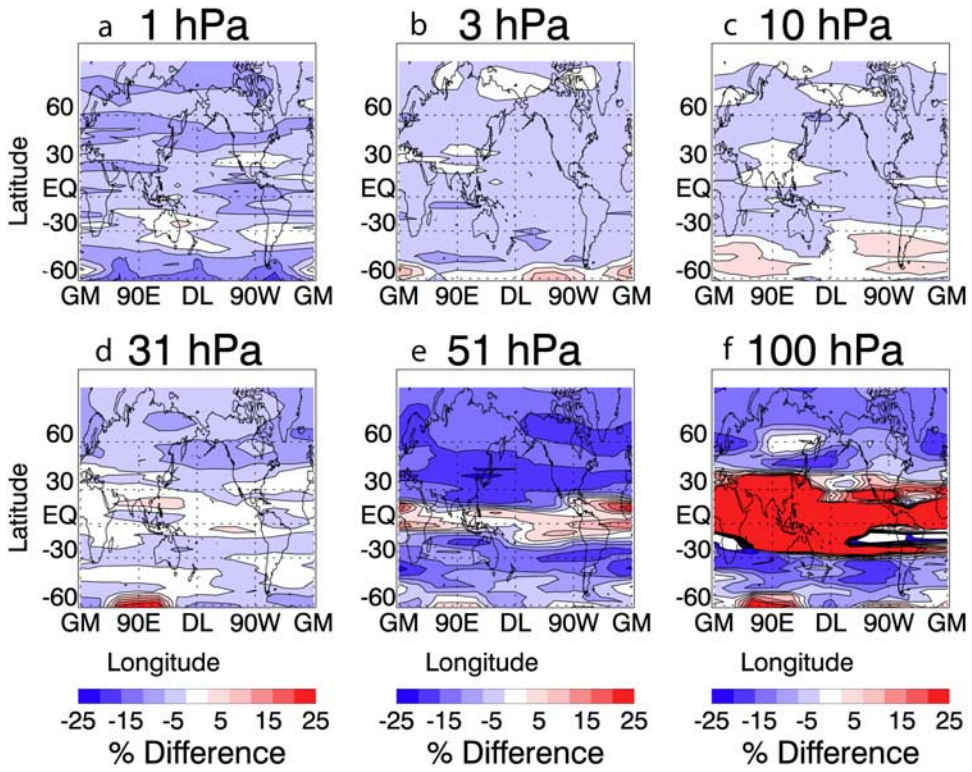

Figure 13. (a–f) Shown are Mercator representations of the ozone percent difference between HIRDLS (v2.04.09) and collocated Microwave Limb Sounder (MLS, v2.2) for 15 July 2006. Each plot corresponds to a pressure level (1, 3, 10, 31, 51, and 100 hPa), as indicated above each plot. The ozone fields from which these differences are calculated are relatively quiescent.

than in the NH is likely due to the fact that most of the SH winter coincidences occurred near the polar vortex where large ozone gradients are common. Some share of the cause may possibly be attributed to obstruction prediction issues alluded to earlier, but this is unlikely as the effect seems to be fairly limited to when the spacecraft traverses the local terminator.

6.2. MLS

[50] In this section HIRDLS ozone is compared to the v2.2 ozone product of Aura-MLS [*Waters et al.*, 2006; *Froidevaux et al.*, 2006]. MLS data were screened on the basis of quality, status, and threshold values listed at http://mls.jpl.nasa.gov/data/MLS_v2.2_miniQualityDocument.pdf. MLS was first interpolated to the HIRDLS pressure levels; then HIRDLS and MLS ozone were binned in 2.5-degree latitude by 30-degree longitude bins. Three comparison views are shown: (1) daily Mercator plots of HIRDLS minus MLS ozone differences for six pressure surfaces (Figure 13), (2) zonal-average plots of HIRDLS minus MLS ozone differences for four months (Figure 14), and finally (3) a comparison of HIRDLS and MLS ozone in the winter northern high latitudes through specific geographic regions where there are interesting meteorological conditions (Figure 15). These comparisons show that the overall structure and morphology of ozone features are in excellent agreement with MLS, even in the highly structured winter northern polar region. In addition the HIRDLS bias appears to be very consistent with that found in the comparisons shown earlier.

[51] Figures 13a–13d indicate that HIRDLS ozone is generally within 10% of the MLS values between 1 and 30 hPa, with small exceptions at southern high latitudes, and is within 5% between 3 and 10 hPa. At 50 hPa HIRDLS is 20% low over wide regions in the NH, which is consistent with the ACE comparison and a number of the lidar and sonde comparisons (SAUNA, WAVES, and OHP). One also starts to see the high bias at low latitudes at this pressure level, which is probably caused by the onset of the cloud-related spikes. At 100 hPa, HIRDLS has a bias of 15–20% or less at middle and high latitudes, and a very high positive bias at low latitudes. This high bias region is saturated in the plot at above 25% and is actually closer to about 100% or more, as was observed with the low-latitude SHADOZ ozonesondes.

[52] Figure 14 shows the zonal-mean HIRDLS minus MLS ozone difference, for 4 months at different times of the year. Different numbers of days went into the zonal averages for each of these months, ranging from 4 to 25 days, but this does not have a big effect on the magnitude of the resulting differences, indicating they are relatively stable. These plots confirm many of the observations that were made with the other comparisons. Among these observations are (1) a 5–10% low bias seen between roughly 1 and 10 hPa for most latitudes; (2) a small region of ~5% high bias which occurs at 10–30 hPa at all latitudes (consistent with SHADOZ, WAVES, MLO, TMF, and ACE

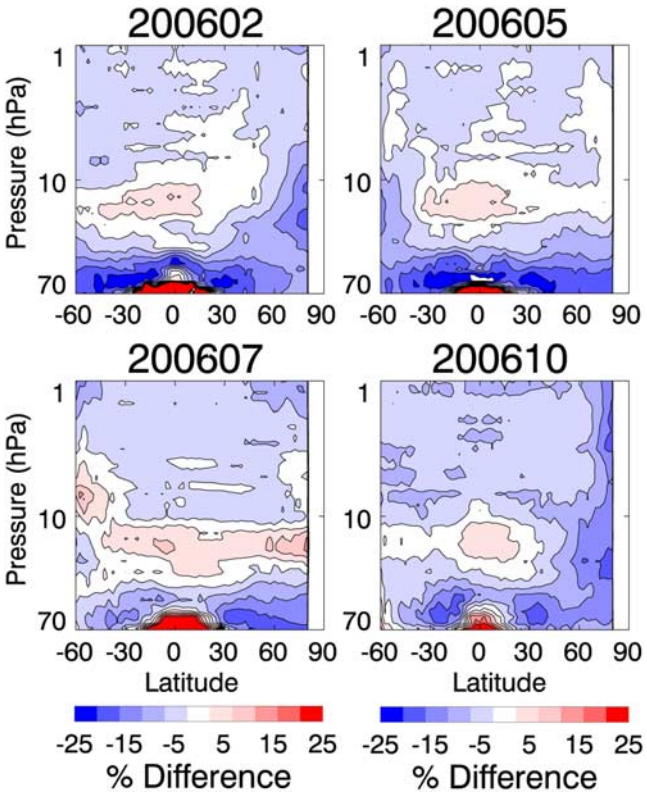

Figure 14. Shown are zonal mean plots of the ozone percent difference between HIRDLS v2.04.09 and collocated MLS v2.2, February (24 days), May (4 days), July (22 days), and October (4 days) of 2006.

comparisons, somewhat less with OHP), except at high southern latitudes, where this occurs at roughly 5 hPa (also seen with the SH ACE comparison); (3) a stronger HIRDLS low bias, approaching 20% or more at midlatitudes, at greater than 50 hPa; and (4) a high HIRDLS bias at low latitudes, beginning at ~50 hPa and increasing rapidly with increasing pressure. The differences between months are not remarkable, except to say that there seems to be a stronger HIRDLS low bias at 50 hPa and greater during February and May compared to July and October.

[53] The analysis summarized in Figure 15 provides a cross validation of HIRDLS with MLS through an interesting geophysical feature in a region where high variability makes limb measurements most difficult. We show that HIRDLS observes decreased levels of ozone inside the polar vortex, and in low-ozone pockets [*Manney et al.*, 1995] that develop in stratospheric anticyclones. Anticyclones have been extensively documented with analysis of solar occultation and MLS ozone data [*Harvey et al.*, 2004, 2008]. Low ozone occurs in the vortex from a combination of strong descent of low ozone from above and confinement of air at high latitudes where polar stratospheric cloud formation is more likely to occur. Low ozone inside the anticyclone develops primarily owing to the latter mechanism [*Morris et al.*, 1995].

[54] Figure 15a shows polar projections of ozone in the Northern Hemisphere, for all 2006 January 17 orbits, measured by HIRDLS (Figure 15, left) and MLS (Figure 15, right), on the 1200 K potential temperature surface (~45 km). The ozone distribution on this day is clearly seen by both HIRDLS and MLS. At this altitude and time of year, ozone maximizes in the tropics and decreases poleward. These maps highlight how, at this level, the concentration of ozone is especially depleted inside both the vortex and the anticyclone. The Arctic vortex (black contour, small area) and the Aleutian anticyclone (white contour, large area) were defined on this day using the algorithm presented by *Harvey et al.* [2002].

[55] The vertical ozone curtain plots in Figure 15b represent one orbital leg (highlighted with black boxes in the polar plot above) that intersects both the vortex and the Aleutian anticyclone low-ozone pocket. The anticyclone low-ozone pocket is very well defined above ~900 K (30 km). The orbit segment shown in the curtain plot for each instrument only grazes the edge of the vortex, but slices through the center of the anticyclone, which appears to the right of the vortex. The ozone morphology and magnitudes observed are in remarkable agreement in this region, especially considering that they are not exactly coincident. HIRDLS higher vertical resolution suggests filamentary structure near the base of the pocket that is not captured by MLS.

[56] Figure 15c shows mean and standard deviation of the ozone profiles within the three different air mass types: (1) anticyclone, (2) vortex, and (3) ''ambient'' (air that is neither in the vortex nor in an anticyclone). Profiles equatorward of 50°N are not considered so that the anticyclone category only contains ozone inside the Aleutian high and is not obscured by mixing multiple anticyclones together. Both the anticyclone and vortex ozone profiles show lower ozone mixing ratios throughout the lower and middle stratosphere compared to ambient air in the same latitude range. On this particular day, the lowest ozone is found in the anticyclone. The mean profiles between MLS and HIRDLS agree to within about 10% (HIRDLS ~500 ppbv low) and the standard deviation profiles agree very well. Both instruments show larger ozone variance inside the anticyclone compared to vortex and ambient regions.

7. Summary and Discussion

[57] Overall, comparisons of HIRDLS ozone with ozone measured with ground-based and airborne lidar, ozonesondes, and other satellite instruments show very good agreement; remarkably good when considering that more than 80% of the aperture is obstructed. An estimate of the HIRDLS ozone precision is 5–10% between 1 and 50 hPa, based on the variability of HIRDLS measurements in regions of minimum geophysical variability.

[58] Comparisons with correlative data sources indicate that HIRDLS ozone is recoverable between 1 hPa and 100 hPa at middle and high latitudes and between 1 and 50 hPa at low latitudes. The majority of the comparisons show that HIRDLS ozone accuracy is better than 10% between 1 and 30 hPa (HIRDLS biased generally low). Some lidars indicate that HIRDLS ozone accuracy may by better than 5% between 2 and 10 hPa, and some sonde comparisons indicate only a 5% HIRDLS low bias at pressures as high as 30–40 hPa. A region of positive 5%

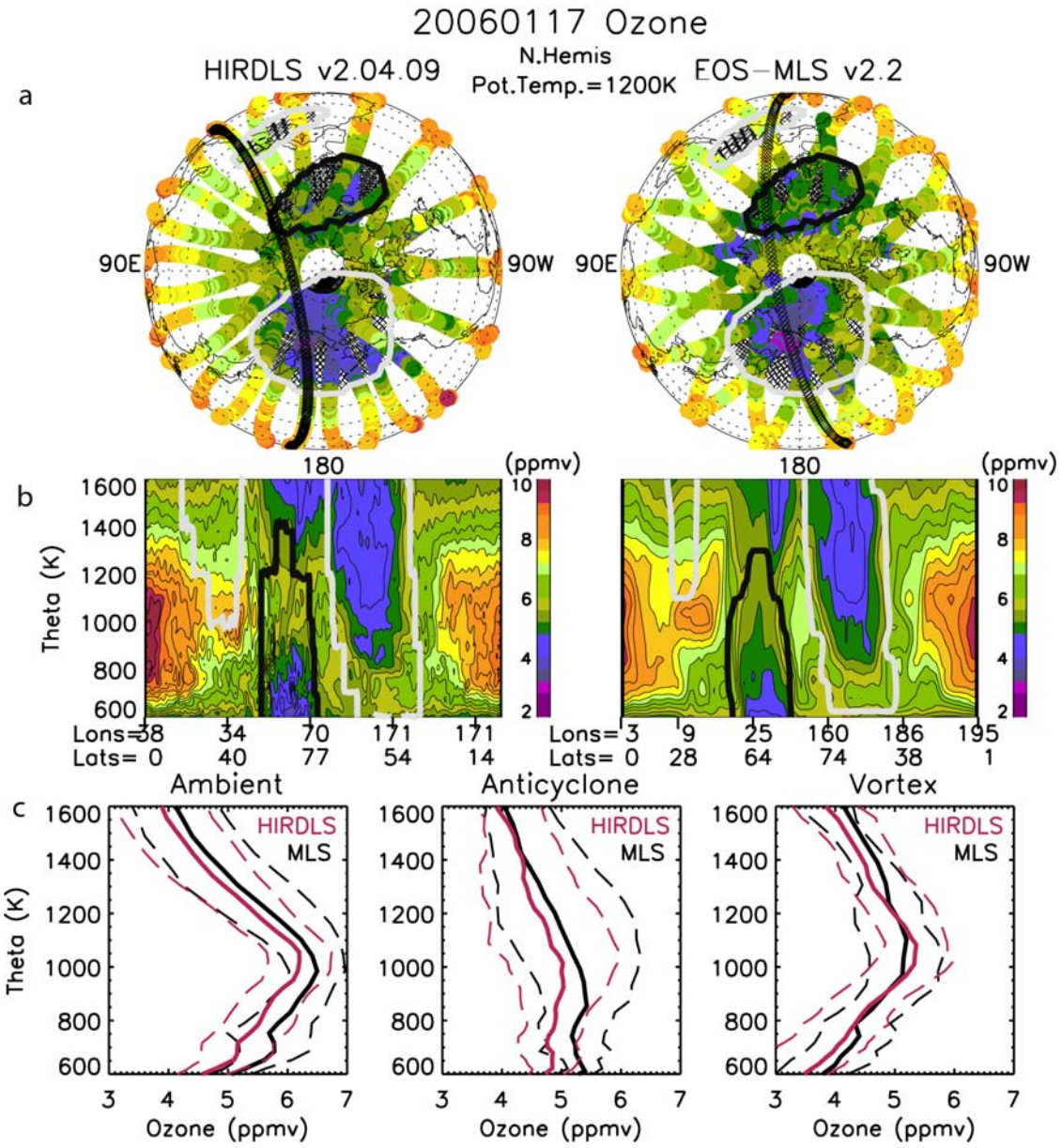

Figure 15. Ozone is compared for an orbit on 17 January 2006 that passes through three types of air masses: anticyclone, vortex, and ''ambient'' air (air that is neither in the vortex nor in the anticyclone). (a) Polar projections of the ozone distributions for HIRDLS and MLS ozone on the 1200 K potential temperature surface (∼45 km). (b) Curtain plots of the swaths indicated by the black boxes in the polar plots. In all four plots the anticyclone and vortex edges are marked in white and black outlines, respectively. (c) Mean and standard deviation ozone profiles within the three different air mass types: ''ambient,'' anticyclone, and vortex, respectively, with MLS in black and HIRDLS in red.

HIRDLS bias exists in a limited pressure range within 10–30 hPa at nearly all latitudes; this is observed by comparisons with sondes (SHADOZ, WAVES), lidars (MLO, TMF) and satellites (ACE, MLS). At high southern latitudes this localized high bias occurs at roughly 5 hPa (ACE, MLS). Between 50 and 100 hPa, at middle and high latitudes, a HIRDLS low bias of 10–20% or more is widely observed. At low latitudes a high HIRDLS bias begins at ∼50 hPa and increases rapidly with increasing pressure. This may be caused by spikes indirectly related to the presence of clouds.

[59] Ozonesonde and lidar profile comparisons give a strong indication that HIRDLS is capable of detecting fine vertical structure in the ozone field on the order of 1 to 2 km. Multiple examples are shown of small-scale features that are captured by both HIRDLS and either sonde or lidar. Comparisons with MLS strongly suggest that HIRDLS is capable of resolving low-ozone pocket features associated with anticyclones in the highly variable northern winter high latitudes. These measurements and comparisons with high-latitude SAUNA sondes suggest HIRDLS resolves highly structured vertical features, but this is difficult to

verify owing to the extreme geophysical variability and the inability to verify that HIRDLS and correlative measurements are sampling the same air masses.

[60] Continuing development of the radiance correction algorithms and of the cloud detection and filtering algorithms may yield further reductions in the systematic bias and an increase in the measurement range earthward to pressures greater than 50–100 hPa.

[61] **Acknowledgments.** This work was supported by NASA contract NAS5-97046.Work at the Jet Propulsion Laboratory, California Institute of Technology, was carried out under a contract with the National Aeronautics and Space Administration. The ACE mission is funded primarily by the Canadian Space Agency. The special efforts made to coordinate measurements with HIRDLS overpasses, by ground teams such as the students of UNA, are greatly appreciated. Finally, this effort would not have been possible had it not been for the administrative support provided in myriad ways by Barb Tunison and Linda Henderson, always in the most professional, kind, and consistent way that one could wish for.

References

Barnes, R. A., A. R. Bandy, and A. L. Torres (1985), Electrochemical concentration cell ozone sonde accuracy and precision, *J. Geophys. Res.*, *90*, 7881–7887.

Bernath, P. F., et al. (2005), Atmospheric Chemistry Experiment (ACE): Mission overview, *Geophys. Res. Lett.*, *32*, L15S01, doi:10.1029/2005GL022386.

Edwards, D. P., J. C. Gille, P. L. Bailey, and J. J. Barnett (1995), Selection of sounding channels for the High Resolution Dynamics Limb Sounder, *Appl. Opt.*, *34*(30), 7006.

Folkins, I., P. Bernath, C. Boone, G. Lesins, N. Livesey, A. M. Thompson, K. Walker, and J. C. Witte (2006), Seasonal cycles of O_3, CO, and convective outflow at the tropical tropopause, *Geophys. Res. Lett.*, *33*, L16802, doi:10.1029/2006GL026602.

Froidevaux, L., et al. (2006), Early validation analysis of atmospheric profiles from EOS MLS on the Aura satellite, *IEEE Trans. Geosci. Remote Sens.*, *44*(5), 1106–1121.

Gille, J. C., and J. J. Barnett (1996), Conceptual design of the High Resolution Dynamics Limb Sounder (HIRDLS), *Proc. SPIE Int. Soc. Opt. Eng.*, *2830*, 190–201.

Gille, J., et al. (2005), Development of special corrective processing of HIRDLS data and early validation, *Proc. SPIE Int. Soc. Opt. Eng.*, *5883*(58830H), 1–11.

Gille, J. C., et al. (2008), The High Resolution Dynamics Limb Sounder (HIRDLS): Experiment overview, results, and temperature validation, *J. Geophys. Res.*, doi:10.1029/2007JD008824, in press.

Godin, S., G. Mégie, and J. Pelon (1989), Systematic lidar measurements of the stratospheric ozone vertical distribution, *Geophys. Res. Lett.*, *16*(6), 547–550.

Godin-Beekmann, S., J. Porteneuve, and A. Garnier (2003), Systematic DIAL ozone measurements at Observatoire de Haute-Provence, *J. Environ. Monit.*, *5*, 57–67.

Harvey, V. L., R. B. Pierce, T. D. Fairlie, and M. H. Hitchman (2002), An object oriented climatology of stratospheric polar vortices and anticyclones, *J. Geophys. Res.*, *107*(D20), 4442, doi:10.1029/2001JD001471.

Harvey, V. L., R. B. Pierce, M. H. Hitchman, C. E. Randall, and T. D. Fairlie (2004), On the distribution of ozone in stratospheric anticyclones, *J. Geophys. Res.*, *109*, D24308, doi:10.1029/2004JD004992.

Harvey, V. L., C. E. Randall, G. L. Manney, and C. S. Singleton (2008), Low-ozone pockets observed by EOS-MLS, *J. Geophys. Res.*, doi:10.1029/2007JD009181, in press.

Johnson, B. J., S. J. Oltmans, D. J. Hofmann, and J. A. Lathrop (1998), Evaluation of ECC ozone sonde performance from recent field and laboratory intercomparisons, in *Proceedings of the XVIII Quadrennial Ozone Symposium, L'Aquila, Italy, 12–21 September 1996*, edited by R. Bojkov and G. Visconti, pp. 927–930, Parco Sci. e Tecnol. d'Abruzzo, Italy.

Johnson, B. J., S. J. Oltmans, H. Vömel, H. G. J. Smit, T. Deshler, and C. Kroger (2002), Electrochemical concentration cell (ECC) ozonesonde pump efficiency measurements and tests on the sensitivity to ozone of buffered and unbuffered ECC sensor cathode solutions, *J. Geophys. Res.*, *107*(D19), 4393, doi:10.1029/2001JD000557.

Kerzenmacher, T. E., et al. (2005), Measurements of O_3, NO_2 and temperature during the 2004 Canadian Arctic ACE Validation Campaign, *Geophys. Res. Lett.*, *32*, L16S07, doi:10.1029/2005GL023032.

Leblanc, T., I. S. McDermid, A. Hauchecorne, and P. Keckhut (1998), Evaluation of optimization of lidar analysis algorithms using simulated data, *J. Geophys. Res.*, *103*(D6), 6177–6187.

Liu, X., K. Chance, C. E. Sioris, T. P. Kurosu, and M. J. Newchurch (2006), Intercomparison of GOME, ozonesonde, and SAGE II measurements of ozone: Demonstration of the need to homogenize available ozonesonde data sets, *J. Geophys. Res.*, *111*, D14305, doi:10.1029/2005JD006718.

Logan, J. A., et al. (1999), Trends in the vertical distribution of ozone: A comparison of two analyses of ozonesonde data, *J. Geophys. Res.*, *104*(D21), 26,373–26,400.

Manney, G. L., L. Froidevaux, J. W. Waters, R. W. Zurek, J. C. Gille, J. B. Kumer, J. L. Mergenthaler, A. E. Roche, A. O'Neill, and R. Swinbank (1995), Formation of low-ozone pockets in the middle stratospheric anticyclone during winter, *J. Geophys. Res.*, *100*(D7), 13,939–13,950.

Manney, G. L., et al. (2007), The high Arctic in extreme winters: Vortex, temperature, and MLS and ACE-FTS trace gas evolution, *Atmos. Chem. Phys. Disc.*, *7*, 10,235–10,285.

Massie, S., et al. (2007), High Resolution Dynamics Limb Sounder observations of polar stratospheric clouds and subvisible cirrus, *J. Geophys. Res.*, *112*, D24S31, doi:10.1029/2007JD008788.

McDermid, I. S., S. M. Godin, and L. O. Lindqvist (1990), Ground-based laser DIAL system for long-term measurements of stratospheric ozone, *Appl. Opt.*, *29*, 3603–3612.

McDermid, I. S., T. D. Walsh, A. Deslis, and M. L. White (1995), Optical-systems design for a stratospheric lidar system, *Appl. Opt.*, *34*, 6201–6210.

McDermid, I. S., G. Beyerle, D. A. Haner, and T. Leblanc (2002), Redesign and improved performance of the JPL-TMF tropospheric ozone lidar, *Appl. Opt.*, *41*, 7550–7555.

McGee, T. J., M. Gross, R. Ferrare, W. S. Heaps, and U. N. Singh (1993), Raman DIAL measurements of stratospheric ozone in the presence of volcanic aerosols, *Geophys. Res. Lett.*, *20*, 955–958.

Morris, G. A., et al. (1995), Trajectory mapping and applications to data from the Upper Atmosphere Research Satellite, *J. Geophys. Res.*, *100*(D8), 16,491–16,506.

Randall, C. E., V. L. Harvey, C. S. Singleton, P. F. Bernath, C. D. Boone, and J. U. Kozyra (2006), Enhanced NO_x in 2006 linked to strong upper stratospheric Arctic vortex, *Geophys. Res. Lett.*, *33*, L18811, doi:10.1029/2006GL027160.

Smit, H. G. J., et al. (2007), Assessment of the performance of ECC-ozonesondes under quasi-flight conditions in the environmental simulation chamber: Insights from the Juelich Ozone Sonde Intercomparison Experiment (JOSIE), *J. Geophys. Res.*, *112*, D19306, doi:10.1029/2006JD007308.

Thompson, A. M., et al. (2003a), Southern Hemisphere Additional Ozonesondes (SHADOZ) 1998–2000 tropical ozone climatology: 1. Comparison with Total Ozone Mapping Spectrometer (TOMS) and ground-based measurements, *J. Geophys. Res.*, *108*(D2), 8238, doi:10.1029/2001JD000967.

Thompson, A. M., et al. (2003b), Southern Hemisphere Additional Ozonesondes (SHADOZ) 1998–2000 tropical ozone climatology: 2. Tropospheric variability and the zonal wave-one, *J. Geophys. Res.*, *108*(D2), 8241, doi:10.1029/2002JD002241.

Thompson, A. M., J. C. Witte, H. G. J. Smit, S. J. Oltmans, B. J. Johnson, V. W. J. H. Kirchhoff, and F. J. Schmidlin (2007), Southern Hemisphere Additional Ozonesondes (SHADOZ) 1998–2004 tropical ozone climatology: 3. Instrumentation, station-to-station variability, and evaluation with simulated flight profiles, *J. Geophys. Res.*, *112*, D03304, doi:10.1029/2005JD007042.

Walker, K. A., C. E. Randall, C. R. Trepte, C. D. Boone, and P. F. Bernath (2005), Initial validation comparisons for the Atmospheric Chemistry Experiment (ACE-FTS), *Geophys. Res. Lett.*, *32*, L16S04, doi:10.1029/2005GL022388.

Waters, J. W., et al. (2006), The Earth Observing System Microwave Limb Sounder (EOS MLS) on the Aura satellite, *IEEE Trans. Geosci. Remote Sens.*, *44*(5), 1075–1092.

J. J. Barnett and C. L. Hepplewhite, Department of Physics, University of Oxford, Oxford OX1 2JD, UK.

P. F. Bernath, C. D. Boone, and K. A. Walker, Department of Chemistry, University of Waterloo, Waterloo, ON, Canada N2L 3G1.

B. R. Bojkov, T. J. McGee, L. W. Twigg, and D. N. Whiteman, NASA Goddard Space Flight Center, Greenbelt, MD 20771, USA.

C. Cavanaugh, M. T. Coffey, C. Craig, T. D. Eden, G. Francis, J. C. Gille, C. Halvorson, J. W. Hannigan, R. Khosravi, D. E. Kinnison, H. Lee, S. T. Massie, B. Nardi, and D. Packman, National Center for Atmospheric Research, Boulder, CO 80301, USA. (nardi@ucar.edu)

J. Craft, V. Dean, C. Krinsky, J. Loh, B. Torpy, and G. Young, Center for Limb Atmospheric Sounding, University of Colorado, Boulder, CO 80309, USA.

L. Froidevaux and A. Lambert, Jet Propulsion Laboratory, Pasadena, CA 91109, USA.

S. Godin-Beekmann, Service d'Aéronomie/IPSL, CNRS, Université Pierre et Marie Curie, UMR 7620, Service d'Aéronomie, F-75005 Paris, France.

V. L. Harvey and C. E. Randall, Laboratory for Atmospheric and Space Physics, Boulder, CO 80303, USA.

T. Leblanc and I. S. McDermid, Table Mountain Facility, Jet Propulsion Laboratory, California Institute of Technology, Wrightwood, CA 92397, USA.

W. J. Reburn and A. Waterfall, Rutherford Appleton Laboratory, Didcot OX11 0QX, UK.

A. M. Thompson, Department of Meteorology, Pennsylvania State University, University Park, PA 16802, USA.

J. Valverde-Canossa, Laboratorio de Quimica de Atmosfera, Universidad Nacional, Apartado 86, Heredia, 3000 Costa Rica.

J. C. Witte, Science Systems and Applications, Inc., Lanham, MD 20706, USA.